Eur. Phys. J. Plus (2018) **133**: 557
DOI 10.1140/epjp/i2018-12360-y

THE EUROPEAN PHYSICAL JOURNAL PLUS

Regular Article

# Self-excited and hidden attractors in a novel chaotic system with complicated multistability

Hayder Natiq[1], M.R.M. Said[1,2,3], M.R.K. Ariffin[1,3], Shaobo He[6], Lamberto Rondoni[3,4,5], and Santo Banerjee[1,3,a]

[1] Institute for Mathematical Research, Universiti Putra Malaysia, Serdang, Malaysia
[2] Department of Mathematics, Universiti Putra Malaysia, Serdang, Malaysia
[3] Malaysia-Italy Centre of Excellence for Mathematical Science, Universiti Putra Malaysia, Serdang, Malaysia
[4] Dipartimento di Scienze Matematiche and Graphene@Polito Lab, Politecnico di Torino, Turin, Italy
[5] INFN, Sezione di Torino, Via Pietro Giuria 1, 10125 Torino, Italy
[6] School of Physics and Electronics, Central South University, Changsha 410083, China

Received: 14 September 2018 / Revised: 29 October 2018
Published online: 31 December 2018
© Società Italiana di Fisica / Springer-Verlag GmbH Germany, part of Springer Nature, 2018

**Abstract.** In this paper, a new 3D chaotic system with trigonometric function term as a nonlinear controller is proposed. Depending on the nonlinear controller and the value of the parameters, the proposed system exhibits self-excited attractor with an unstable equilibrium, and hidden attractor with no equilibrium or a stable equilibrium. In addition, the unusual and striking dynamic behavior of the coexistence of self-excited chaotic with periodic attractors, two self-excited chaotic attractors with periodic attractor, three periodic attractors, hidden chaotic with point attractors, two hidden chaotic attractors, and four hidden chaotic attractors are explored by selecting appropriate initial values. Consequently, the proposed system has high sensitivity to its initial values and parameters, hence it can be applied in chaos-based cryptographic applications. Thus, the non-periodicity of coexisting attractors of the system is investigated through Lyapunov exponents and Sample Entropy. To demonstrate the performance of the system in real applications, we construct a pseudo-random number generator (PRNG) based on the hidden attractor case. The randomness test results show that the generated PRNG pass all the statistical tests.

## 1 Introduction

In 1963, the modern era of chaos theory has been introduced by Lorenz who accidentally discovered the sensitive dependence on initial condition in a set of three coupled first-order ordinary differential equations [1]. During the second half of the last century, further investigations of three-dimensional chaotic systems with simple nonlinearities were motivated by Lorenz system (*e.g.*, Rössler system, Sprott system and Chen system [2–4]). For the past two decades, much attention was given to chaos which has established itself as significant branch of nonlinear dynamics, modern mathematics and physics with many applications in biology and engineering, as well as secure communications [5–8].

Existing chaotic systems can be classified into two categories: systems with self-excited attractors and systems with hidden attractors. The chaotic system with self-excited attractors has a basin of attraction that is intersected with an unstable equilibrium, whereas the chaotic system with hidden attractors has a basin of attraction which does not intersect with any open neighborhoods of equilibria [9]. However, with further investigation of chaos, it was unexpected to find that many chaotic systems have several possible final stable states (attractors) for a given set of parameters. This phenomenon known as multistability or coexisting attractors. More interestingly, multistability has been observed in numerous natural systems and usually plays a crucial role in the performance of systems [10]. The clear evidence of multistability was first manifested experimentally in a Q-switched gas laser [11], since then chaotic systems with multistability have been extensively reported [12–15]. However, multistability, as a new research direction in chaos theory, is still in its infancy. Therefore, the investigation of chaotic systems with multistability requires further research.

Chaos control is an attractive theoretical subject and very important in studying chaotic dynamics and their applications. One of the main motivations of chaos control is to direct a chaotic system to a desired dynamical

[a] e-mail: santoban@gmail.com

**Table 1.** Parameter choices and different attractors of MACS.

| Parameters | $\lvert f(x_1)\rvert$ | Case name | Type of system |
|---|---|---|---|
| $\sigma, \beta, \delta, \alpha > 0$, $\mu = 0$ | $\lvert\cos(x_1)\rvert$ | Case 1 | *Self-excited* attractor with one *unstable* hyperbolic equilibrium. |
| $\sigma, \beta, \delta > 0$, $\alpha = \mu = 0$ | $\lvert\cos(x_1)\rvert$ | Case 2 | *Hidden* attractor with *no* equilibrium |
| $\sigma, \beta > 0, \delta = \alpha > 0$, $\mu > 0$ | $\lvert\sin(x_1)\rvert$ | Case 3 | *Hidden* attractor with one *stable* equilibrium. |

properties, which is known as chaotification or anti-control of chaos [16,17]. In the endeavor of chaotification, many studies have devoted their efforts to enhance chaos using trigonometric functions due to its complex chaotic behavior and bounded solutions. These studies aim to design systems that can generate unusual or complex chaotic behaviors, such as having coexisting attractors [18] and generating autonomous system with no equilibria [19]. Therefore, the endeavor of chaotification to generate a chaotic system with multi-attribute dynamic is a challenging topic.

Recently, many studies have observed that numerous properties of chaotic systems are similar to their counterparts in traditional cryptography [20–24]. However, when chaotic systems are used in cryptographic applications, the security levels of cryptographic schemes are highly dependent on the sensitivity of initial values and parameters of the applied chaotic systems [25,26]. Chaotic systems with coexisting attractors has complex chaotic behaviors and highly sensitivity to both initial values and parameters. Therefore, those systems would be a suitable for cryptographic applications. Meanwhile, those systems also have some weaknesses, for instance it may be tricky to locate the coexisting chaotic attractors.

In this paper, we present a new 3D multi-attribute chaotic system (MACS), which can show self-excited attractors with one unstable equilibrium, hidden attractors with no equilibrium, and hidden attractors with one stable equilibrium. The attractor type of MACS is completely determined by the nonlinear controller term (trigonometric function) and the value of parameters. The MACS generates various types of coexisting behaviors, which means that it has high sensitivity to its initial values and parameters. Therefore, the MACS would be very suitable in cryptographic applications if the initial values and parameters are chosen from the regions of coexisting chaotic attractors. Using the Lyapunov exponents and Sample Entropy, we examine the initial values of MACS that show coexisting chaotic attractors. Consequently, we use MACS to generate PRNG that can pass all statistical tests.

The rest of this paper is organized as follows: Section 2 introduces the 3D Multi-attribute chaotic system (MACS). Section 3 investigates the existence of coexisting attractors in MACS. In sect. 4, we use the MACS to generate PRNG. The conclusions are presented in sect. 5.

## 2 Multi-attribute chaotic system (MACS) and its dynamical properties

This section presents a new simple 3D chaotic system, which is characterized by less that seven terms with two quadratic nonlinearities and a trigonometric function term as nonlinear controller. The new system shows self-excited attractors with an unstable hyperbolic equilibrium, hidden attractors with no equilibrium, and hidden attractors with a stable hyperbolic equilibrium. Thus, the system is named as multi-attribute chaotic system (MACS). Mathematically, it is defined as

$$\begin{cases} \dfrac{\mathrm{d}x_1}{\mathrm{d}t} = -x_2, \\ \dfrac{\mathrm{d}x_2}{\mathrm{d}t} = x_1 + \delta x_2 x_3, \\ \dfrac{\mathrm{d}x_3}{\mathrm{d}t} = \sigma|f(x_1)| - \beta x_2^2 - \alpha x_3 - \mu, \end{cases} \tag{1}$$

where $x_1$, $x_2$, $x_3$ are the state variables, and $\sigma$, $\beta$, $\delta$, $\alpha$, $\mu$ are the constant parameters of the system. In eq. (1), $|f(x_1)|$ is a nonlinear controller, and is given by either $|\cos(x_1)|$ or $|\sin(x_1)|$. It is clear that the system is rotationally symmetric under the transformation $(x_1, x_2, x_3) \longrightarrow (-x_1, -x_2, x_3)$. In addition, the system becomes dissipative when $\alpha > 0$ and the average of $\delta x_3$ signal in a long run is less than $\alpha$.

In table 1, the MACS shows various attractors depending on the nonlinear controller and the choice of its parameters. As an example, case 1 and case 2 show self-excited and hidden chaotic attractors when $\sigma = 17$, $\beta = 0.6$, $\delta = 0.63$, $\mu = 0$ and $\alpha$ equal to 0.2 and 0, respectively, as can be seen in fig. 1(a), (b). Meanwhile, case 3 shows hidden chaotic attractor when $\sigma = 17$, $\beta = 0.3$, $\delta = \alpha = 0.63$ and $\mu = 0.1$, as is shown in fig. 1(c).

In order to calculate the equilibria of case 1 of MACS, we can choose the parameters $\sigma, \delta, \beta, \alpha > 0$ and $\mu = 0$, then the equilibria can be obtained by solving the following equations:

$$\begin{cases} -x_2 = 0, \\ x_1 + \delta x_2 x_3 = 0, \\ \sigma|\cos(x_1)| - \beta x_2^2 - \alpha x_3 = 0. \end{cases} \tag{2}$$

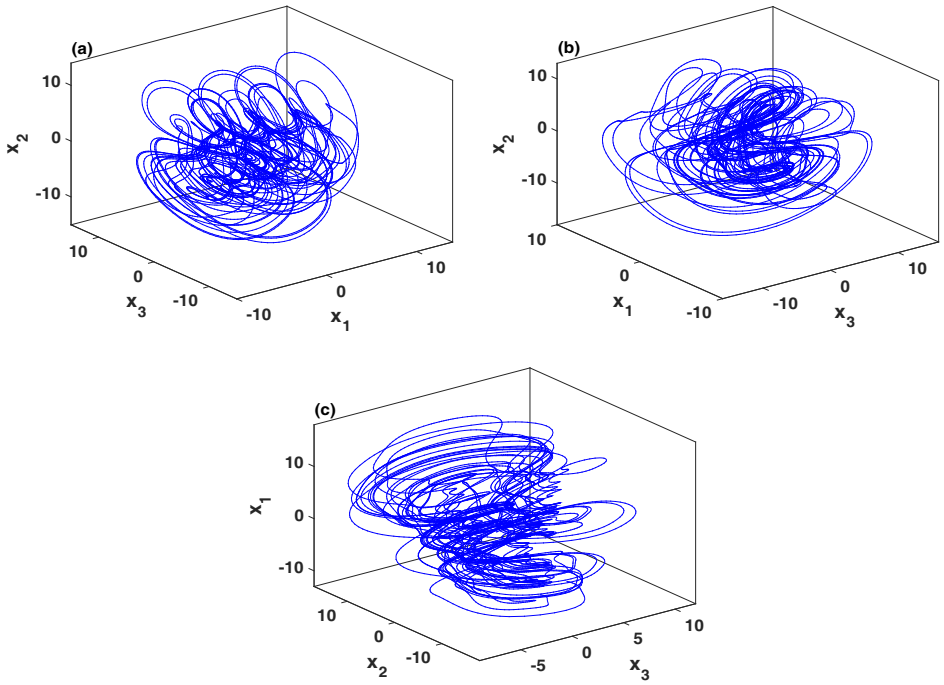


**Fig. 1.** Different perspectives of the MACS cases for the initial values $(0.5, -2, 0)$ with different parameters values: (a) self-excited chaotic attractor with one unstable equilibrium for $\sigma = 17$, $\beta = 0.6$, $\delta = 0.63$, $\mu = 0$ and $\alpha = 0.2$; (b) hidden chaotic attractor with no equilibrium for $\sigma = 17$, $\beta = 0.6$, $\delta = 0.63$, $\mu = 0$ and $\alpha = 0$; (c) hidden chaotic attractor with one stable equilibrium for $\sigma = 17$, $\beta = 0.3$, $\delta = \alpha = 0.63$ and $\mu = 0.1$.

From the above equations, one can observe that case 1 of MACS has only one equilibrium with the following form:

$$E_1 \left(0, 0, \frac{\sigma}{\alpha}\right).$$

The stability of $E_1$ can be studied by computing the corresponding eigenvalues.

Proposition 1. *The equilibrium point $E_1$ of case 1 is*

1) *an unstable saddle-focus point for $\delta^2\sigma^2 < 4\alpha^2$;*
2) *a saddle point for $\delta^2\sigma^2 > 4\alpha^2$.*

*Proof.* For the equilibrium point $E_1$, the Jacobian matrix is given by

$$J_{E_1} = \begin{pmatrix} 0 & -1 & 0 \\ 1 & \dfrac{\delta\sigma}{\alpha} & 0 \\ 0 & 0 & -\alpha \end{pmatrix}.$$

The characteristic equation of Jacobian matrix becomes

$$(\lambda + \alpha)\left(\lambda^2 - \frac{\delta\sigma}{\alpha}\lambda + 1\right) = 0. \tag{3}$$

Consequently, the corresponding eigenvalues are

$$\lambda_1 = -\alpha, \quad \lambda_{2,3} = \frac{\delta\sigma}{2\alpha} \pm \frac{\sqrt{\delta^2\sigma^2 - 4\alpha^2}}{2\alpha}. \tag{4}$$

Since $\sigma$, $\delta$, $\alpha$ are all positive real numbers, it follows that $\lambda_1 < 0$. It can also be shown that if $\delta^2\sigma^2 < 4\alpha^2$, then $\lambda_{2,3}$ have negative square root with positive real values yielding an unstable saddle-focus point. The $\lambda_{2,3}$ have positive real values if $\delta^2\sigma^2 > 4\alpha^2$, hence, $E_1$ is a saddle point. □

In case 2 of MACS, suppose that the parameters $\sigma, \delta, \beta > 0$ and $\alpha = \mu = 0$, then the equilibria are obtained by solving the following equations:

$$\begin{cases} -x_2 = 0, \\ x_1 + \delta x_2 x_3 = 0, \\ \sigma|\cos(x_1)| - \beta x_2^2 = 0. \end{cases} \tag{5}$$

Obviously, the last equation of system (5) is inconsistent since $\sigma > 0$. Thus, there is no equilibrium in system (5).

In case 3 of MACS, we can choose the parameters $\sigma, \beta, \mu > 0$ and $\delta = \alpha > 0$, then the equilibria are obtained by solving the following equations:

$$\begin{cases} -x_2 = 0, \\ x_1 + \delta x_2 x_3 = 0, \\ \sigma|\sin(x_1)| - \beta x_2^2 - \delta x_3 - \mu = 0. \end{cases} \tag{6}$$

Thus, case 3 of MACS has only one equilibrium with the following form:

$$E_2\left(0, 0, \frac{-\mu}{\delta}\right).$$

The corresponding Jacobian matrix of case 3 is given by

$$J = \begin{pmatrix} 0 & -1 & 0 \\ 1 & \delta x_3 & \delta x_2 \\ \dfrac{\sigma \sin(x_1)\cos(x_1)}{|\sin(x_1)|} & -2\beta x_2 & -\delta \end{pmatrix}.$$

It is clear that $\frac{\partial f_3}{\partial_{x_1}} = \frac{\sigma \sin(x_1)\cos(x_1)}{|\sin(x_1)|}$ is undefined at $E_2$. Therefore, stability in the sense of Lyapunov can be used to determine the stability of $E_2$.

An equilibrium point $E$ of a system is said to be Lyapunov stable if and only if for any $\epsilon > 0$ there exists a $\psi > 0$ such that the orbit $\theta(t, E^*)$ of the system satisfies the following relation

$$\|E^* - E\| < \psi \Longrightarrow \|\theta(t, E^*) - E\| < \epsilon.$$

Then, the equilibrium point $E$ is asymptotically stable if the orbit $\theta(t, E^*)$ approach to $E$ as $t \longrightarrow \infty$ [27].

Different initial values, which are close to $E_2$, are used to investigate the stability of $E_2$ in the sense of Lyapunov. As can be seen in fig. 2(a)–(d), $E_2$ is asymptotically stable in the sense of Lyapunov when the parameters $\sigma = 17$, $\delta = 0.63$, $\beta = 0.2$, $\mu = 0.3$ with the initial values $(0 \pm 0.02, 0 \pm 0.02, \frac{-\mu}{\delta} \pm 0.02)$. Meanwhile, the hidden chaotic attractors with Lyapunov exponents $(0.1438, 0, -0.4714)$ can be observed by choosing the initial values $(0+1, 0+1, \frac{-\mu}{\delta} + 1)$ which are not in the stable manifold of $E_2$, as shown in fig. 2(e), (f).

## 3 Various kinds of multistability behaviors

Multistability or coexisting attractors basically means that a system has two or more solutions simultaneously under the same set of parameters and different initial values. In this section, through numerical simulations, extremely multistability behaviors of self-excited and hidden attractors of the MACS are investigated by means of phase portraits, Lyapunov exponents, Kaplan-Yorke dimension, and bifurcation diagram.

When we set $\sigma = 17$, $\delta = 0.63$ with $0.2 \leq \beta \leq 2$, the coexisting bifurcation models of the state variable $x_1$ of case 1 are depicted in fig. 3(a), in which the orbits of system are initiated with the initial values $(2, -2, -1)$ (blue), $(1.8, 0.3, 0)$ (red), $(-1.8, 0.3, 0)$ (black) and $(0.5, -2, 0)$ (green). It can be seen that case 1 of MACS experiences coexisting periodic with chaotic attractors, coexisting multiple chaotic attractors with a periodic orbit, and coexisting three periodic orbits, which occurred when $\beta = 0.47$, $\beta = 1.4$, $\beta = 1.93$, respectively. To further show the interesting nonlinear phenomenon of these multistability behaviors, the corresponding phase portraits are depicted in fig. 4. As can be seen, the coexistence of limit cycle with self-excited chaotic attractors, the coexistence of multiple self-excited chaotic attractors with the symmetric limit cycle, and the coexistence of three limit cycles can be observed in fig. 4(a)–(c), (d)–(f), and (g)–(i), respectively. Additionally, the dynamical properties of attractors in fig. 4 including Lyapunov exponents and Kaplan-Yorke dimension are summarized in table 2.

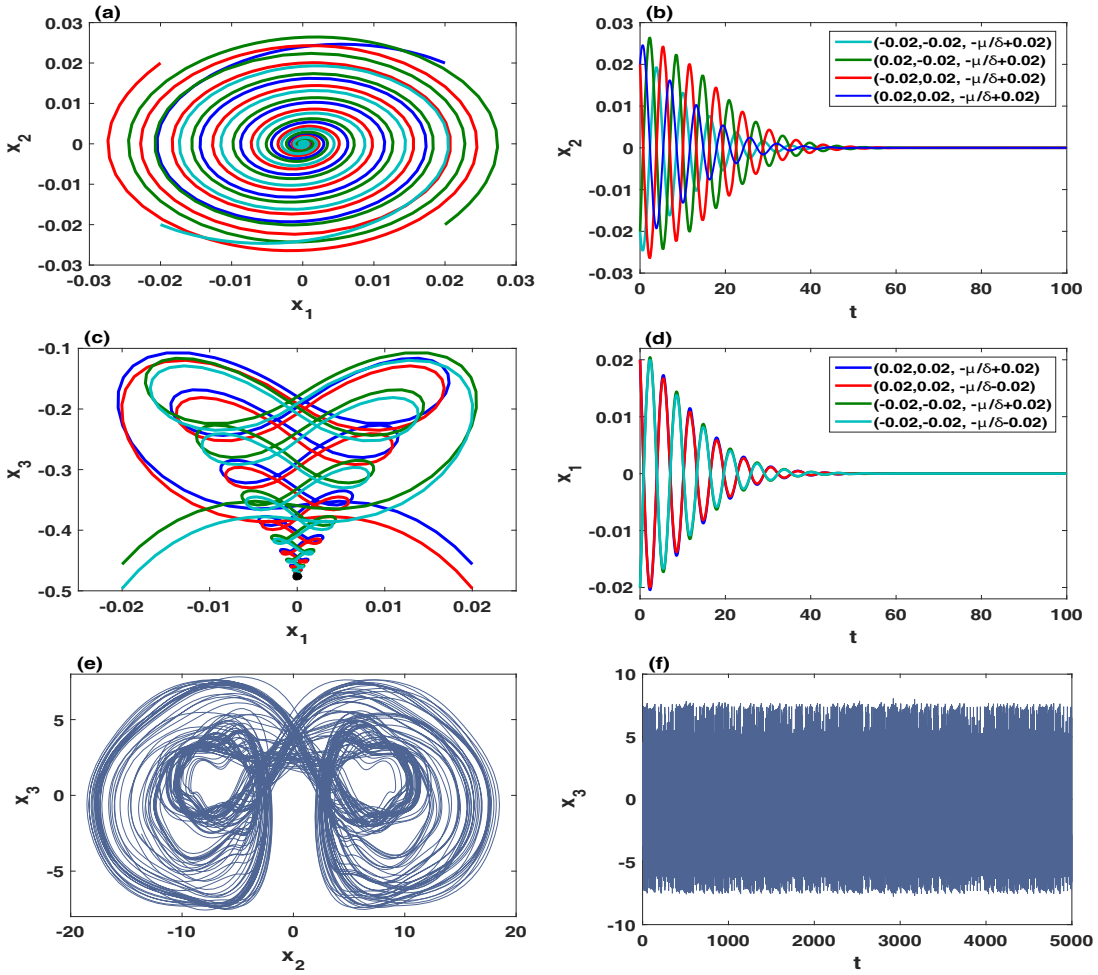


**Fig. 2.** Stability of $E_2$ in the sense of Lyapunov when the parameters $\sigma = 17$, $\delta = 0.63$, $\beta = 0.2$ and $\mu = 0.3$: (a)–(d) asymptotically stability of $E_2$ for different directions of the initial values $(0 \pm 0.02, 0 \pm 0.02, \frac{-\mu}{\delta} \pm 0.02)$; (e), (f) hidden chaotic attractors with the stable equilibrium $E_2$ for the initial values $(0 + 1, 0 + 1, \frac{-\mu}{\delta} + 1)$.

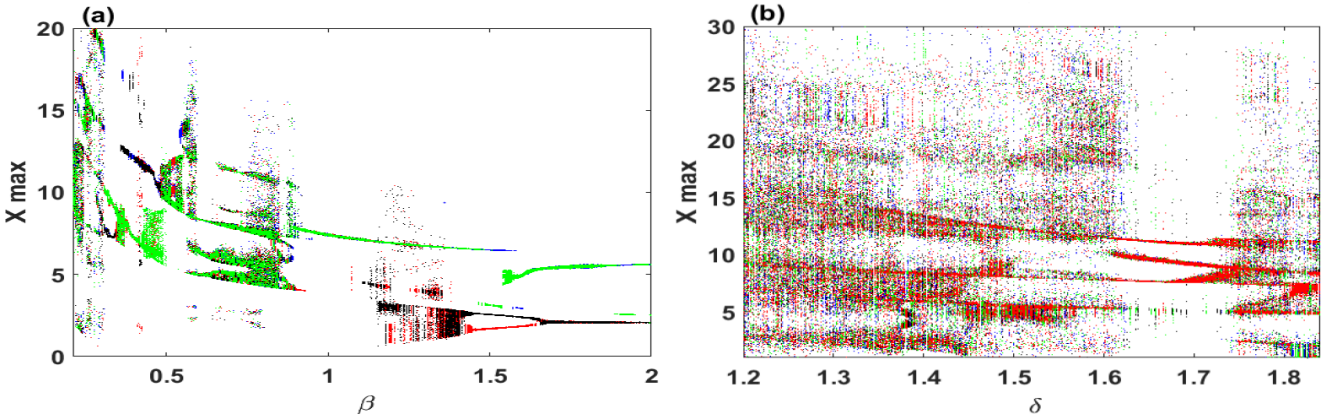


**Fig. 3.** Bifurcation diagrams for the parameters $\beta$ and $\delta$ to illustrate the coexisting attractors: (a) the four coexisting attractors of case 1 where $\sigma = 17$, $\delta = 0.63$, $\alpha = 0.5$ for the initial values $(2, -2, -1)$ (blue), $(1.8, 0.3, 0)$ (red), $(-1.8, 0.3, 0)$ (black) and $(0.5, -2, 0)$ (green); (b) the four coexisting attractors of case 2 when $\sigma = 12$, $\beta = 0.1$ and for the initial values $(1.8, 0.3, 0)$ (blue), $(-1.8, 0.3, 0)$ (red), $(5, 0, -5)$ (black) and $(5, 3, -3)$ (green).

Furthermore, fig. 3(b) depicts the coexisting bifurcation models of the state variable $x_1$ of case 2 of MACS when $\sigma = 12$, $\beta = 0.1$ and $1.2 \leq \delta \leq 1.85$. Meanwhile, the orbits of the system are initiated with the initial values $(1.8, 0.3, 0)$ (blue), $(-1.8, 0.3, 0)$ (red), $(5, 0, -5)$ (black) and $(5, 3, -3)$ (green). It can be seen that case 2 of MACS, respectively, experiences coexisting four hidden chaotic attractor, coexisting four periodic attractors, and then coexisting four

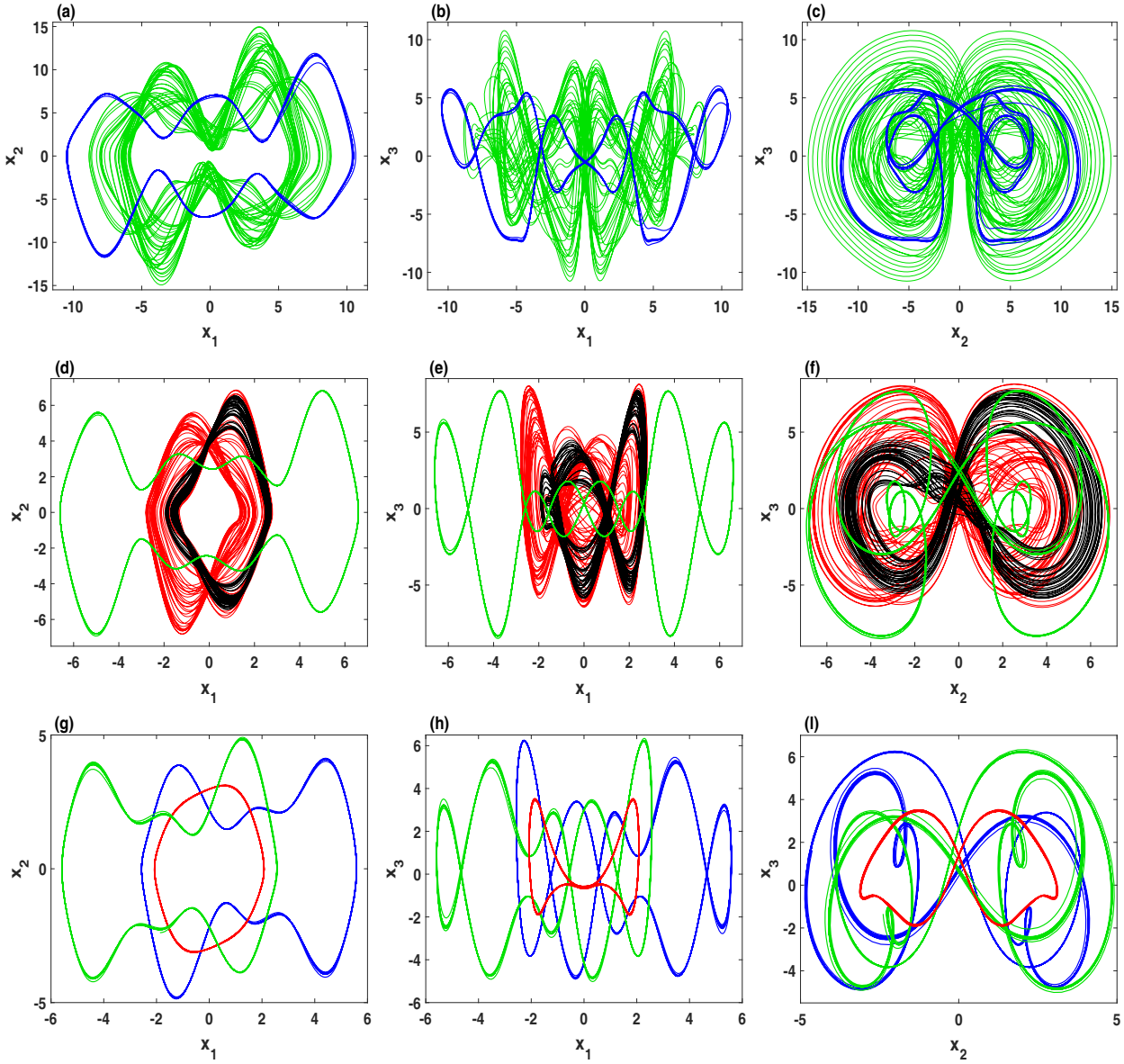


**Fig. 4.** Two and three coexisting attractors of case 1 with the parameters $\sigma = 17$, $\delta = 0.63$, $\alpha = 0.5$ and for the initial values $(2, -2, -1)$ (blue), $(1.8, 0.3, 0)$ (red), $(-1.8, 0.3, 0)$ (black) and $(0.5, -2, 0)$ (green): (a)–(c) the limit cycle and chaotic attractor coexist when $\beta = 0.47$; (d)–(f) the symmetric limit cycle and two chaotic attractors coexist when $\beta = 1.4$; (g)–(i) the three limit cycles coexist when $\beta = 1.93$.

hidden chaotic attractors. To show the complicated dynamic of coexisting different hidden chaotic attractors visually, fig. 5 depicts the corresponding phase portraits when the bifurcation parameter $\delta$ is set as 1.82. As can be seen from fig. 5, four symmetric hidden chaotic attractors coexist for a given set of parameters and different initial values. In addition, the characteristics properties of attractors in fig. 5 are shown in table 2.

For case 3 of MACS, as can be seen, fig. 2 shows the coexistence of hidden chaotic attractor with point attractor for a given set of parameters and different initial values. Furthermore, by selecting the parameters $\sigma = 17$, $\delta = 0.63$, $\beta = 0.3$ and $\mu = 0.3$, multiple hidden chaotic attractors coexist for different initial values, in which the orbit colored in green is initiated with $(1, -1, 1)$ and the orbit colored in black is initiated with $(1, -1, -4)$, as shown in fig. 6. The Lyapunov exponents and Kaplan-Yorke dimension of these coexisting attractors, which appeared in fig. 6, are demonstrated in table 2.

Through the above analysis, we can observe the interesting and appealing multistability phenomenon of the three cases of MACS including coexisting self-excited chaotic with limit cycle, coexisting two self-excited chaotic attractors with symmetric limit cycle, and three limit cycles. In addition, the coexistence of hidden chaotic with point attractors, the coexistence of two hidden chaotic attractors, and the coexistence of four hidden chaotic attractors. Therefore, it can be concluded that the MACS has high sensitivity to both initial values and parameters.

**Table 2.** Details of the coexisting attractors shown in figs. 4, 5 and 6.

| Name | Parameters | Initial values | Lyapunov exponents | KY dimension | Attractor type | Figure |
|---|---|---|---|---|---|---|
| Case 1 | $\beta = 0.47$ | $(2, -2, -1)$ (blue) | $(0, -0.1095, -0.1108)$ | 2.0 | limit cycle | Fig. 4(a)–(c) |
| | | $(0.5, -2, 0)$ (green) | $(0.0784, 0, -0.2598)$ | 2.3018 | S-E C attractor | |
| Case 1 | $\beta = 1.4$ | $(1.8, 0.3, 0)$ (red) | $(0.0886, 0, -0.2594)$ | 2.3416 | S-E C attractor | Fig. 4(d)–(f) |
| | | $(-1.8, 0.3, 0)$ (black) | $(0.0885, 0, -0.2600)$ | 2.3404 | S-E C attractor | |
| | | $(0.5, -2, 0)$ (green) | $(0, -0.1301, -0.1311)$ | 2.0 | limit cycle | |
| Case 1 | $\beta = 1.93$ | $(2, -2, -1)$ (blue) | $(0, -0.1096, -0.1899)$ | 2.0 | limit cycle | Fig. 4(g)–(i) |
| | | $(1.8, 0.3, 0)$ (red) | $(0, -0.1312, -0.1317)$ | 2.0 | limit cycle | |
| | | $(0.5, -2, 0)$ (green) | $(0, -0.1098, -0.1898)$ | 2.0 | limit cycle | |
| Case 2 | $\delta = 1.82$ | $(1.8, 0.3, 0)$ (blue) | $(0.2085, 0, -0.2645)$ | 2.7883 | H C attractor | Fig. 5(a)–(c) |
| | | $(-1.8, 0.3, 0)$ (red) | $(0.1704, 0, -0.2207)$ | 2.7721 | H C attractor | |
| | | $(5, 0, -5)$ (black) | $(0.2514, 0, -0.3782)$ | 2.6647 | H C attractor | |
| | | $(5, 3, -3)$ (green) | $(0.1535, 0, -0.2028)$ | 2.7569 | H C attractor | |
| Case 3 | $\beta = 0.3$ | $(1, -1, 1)$ (green) | $(0.0259, 0, -0.0415)$ | 2.6241 | H C attractor | Fig. 6(a)–(c) |
| | | $(1, -1, -4)$ (black) | $(0.0350, 0, -0.3053)$ | 2.1146 | H C attractor | |

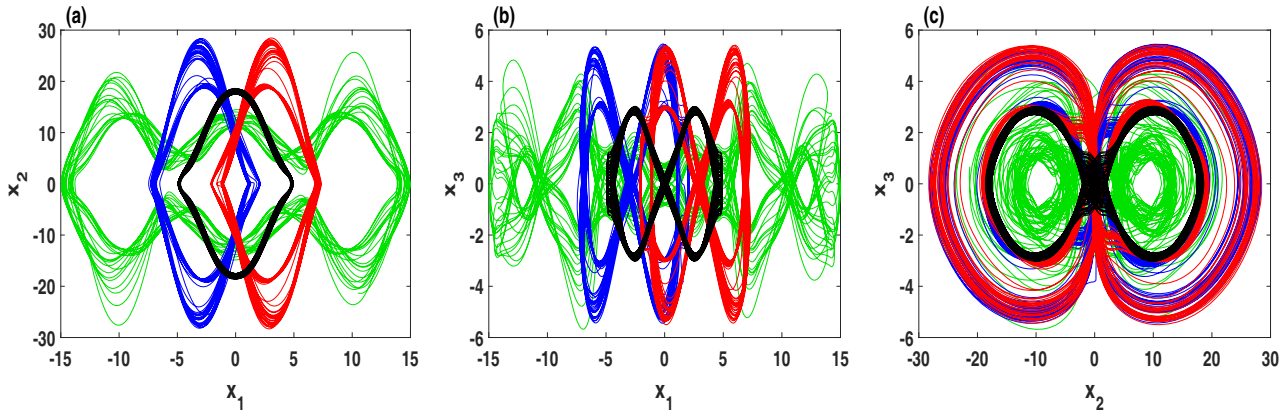


**Fig. 5.** Four coexisting attractors of case 2 with the parameters $\sigma = 12$, $\beta = 0.1$, $\delta = 1.82$ and for the initial values $(1.8, 0.3, 0)$ (blue) and $(-1.8, 0.3, 0)$ (red), $(5, 0, -5)$ (black) and $(5, 3, -3)$ (green).

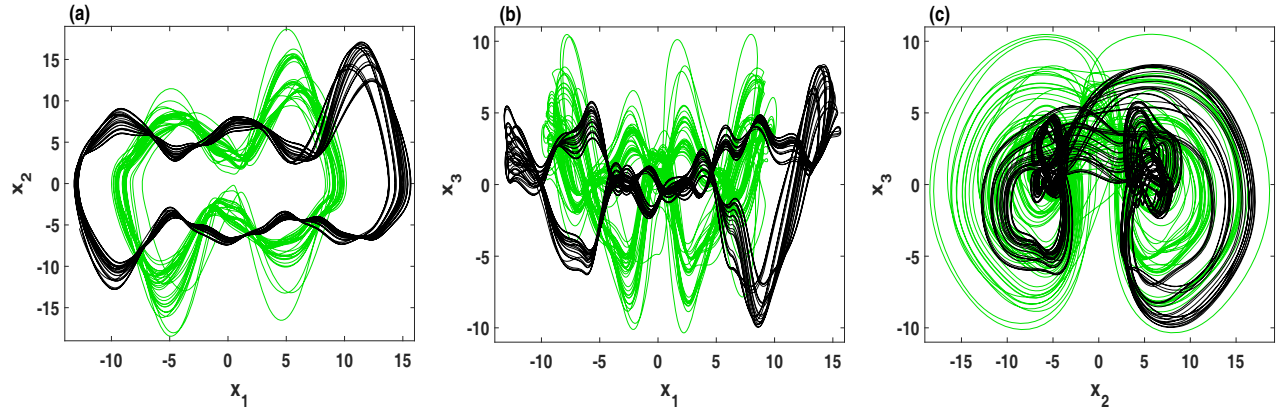


**Fig. 6.** Two coexisting chaotic attractors of case 3 when the parameters $\sigma = 17$, $\delta = 0.63$, $\beta = 0.3$, $\mu = 0.3$ for the initial values $(1, -1, 1)$ (green) and $(1, -1, -4)$ (black).

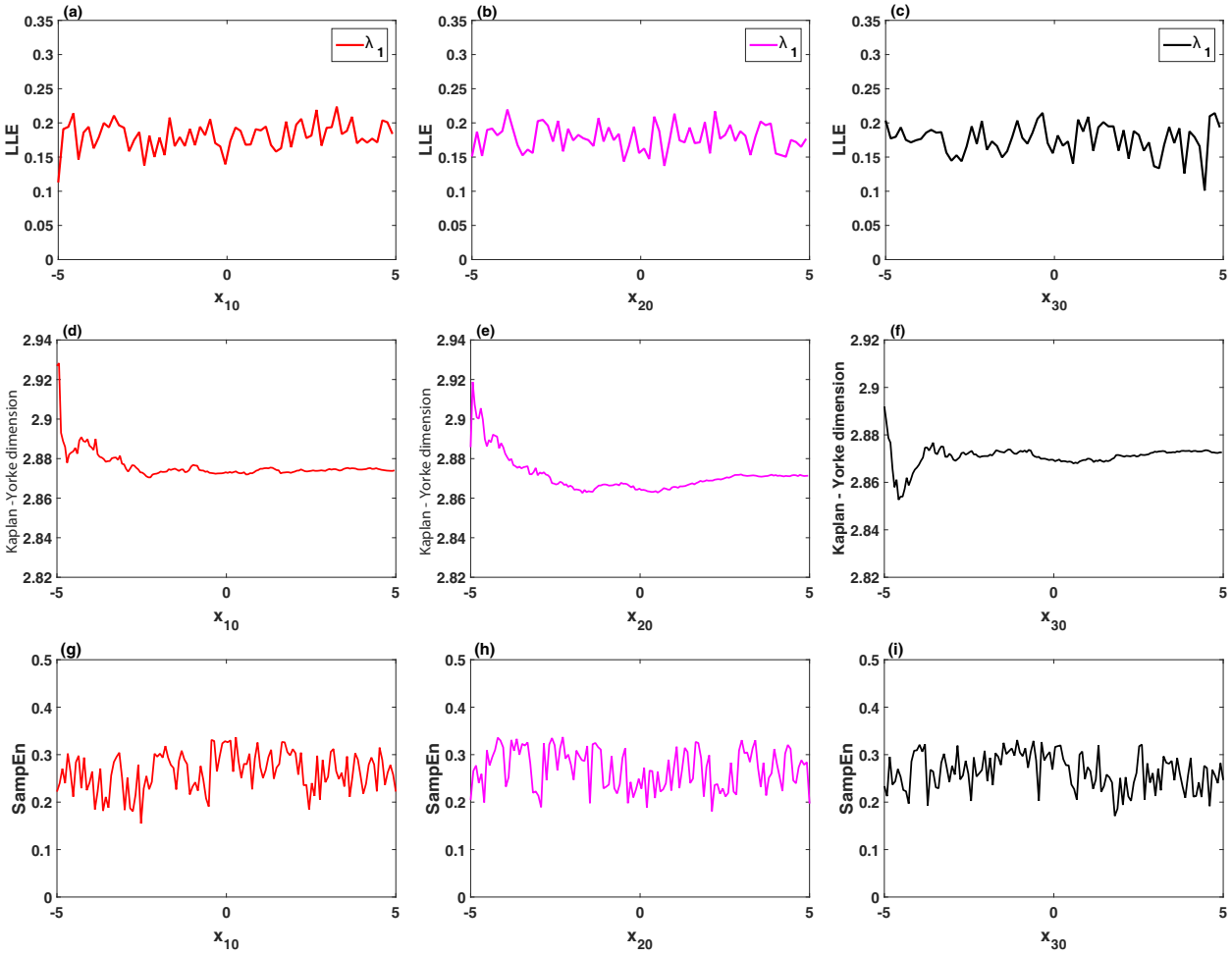


**Fig. 7.** Largest Lyapunov exponents, Kaplan-Yorke dimension and SamEn *versus* varying one of the initial values of case 2 with the parameters $\sigma = 12$, $\delta = 1.2$, $\beta = 0.1$: (a), (d), (g) $(x_{10}, 1, 1)$; (b), (e), (h) $(1, x_{20}, 1)$; (c), (f), (i) $(1, 1, x_{30})$.

## 4 Chaos-based PRNG

The need of pseudo-random number generator (PRNG) arises in many cryptographic applications, *e.g.*, common cryptosystems employ keys, data hiding, and auxiliary quantities used in generating digital signatures [28]. Recently, chaotic systems are used as seeds to produce PRNG. A chaotic system can generate a good PRNG if it has some properties such as highly sensitivity to initial values and parameter, good complexity performance, and high randomness. In the previous section, the highly sensitivity of the MACS has observed by producing various types of coexisting attractors via changing its initial values. In terms of cryptographic applications, such systems might be inappropriate if the PRNG generates from the regions of coexisting chaotic with periodic attractors. Therefore, it can be concluded that we need to find the initial values and parameters that show coexisting chaotic attractors. Consequently, this section discusses how to construct PRNG based on case 2 of MACS, as an example.

### 4.1 Lyapunov exponents and Kaplan-Yorke dimension

As aforementioned, to generate PRNG from case 2 of MACS, firstly, we need to determine the parameters that show coexisting chaotic attractors. As can be seen in fig. 3(b), case 2 shows coexisting chaotic attractors in various values of the parameter $\delta$. In our experiments, we choose $\delta = 1.2$ which produces chaotic behavior for the four selected initial values. However, the behavior of case 2 *versus* varying one and two of initial values are investigated to examine broad range of the initial values. The Largest Lyapunov exponents (LLE) and Kaplan-Yorke dimension *versus* varying one of the initial value in the range of $[-5, 5]$, are calculated and the results are depicted in fig. 7(a)–(c) and (d)–(f), respectively. Furthermore, fig. 8(a)–(c) depict the LLE based contour plots when two of the initial values are varying simultaneously in the range of $[-5, 5]$ with step size of 0.1, meanwhile, the other initial value is fixed as 1. These two figures indicate that case 2 shows fractional dimension chaotic or coexisting chaotic attractors when one or even two of initial values varying in the range of $[-5, 5]$.

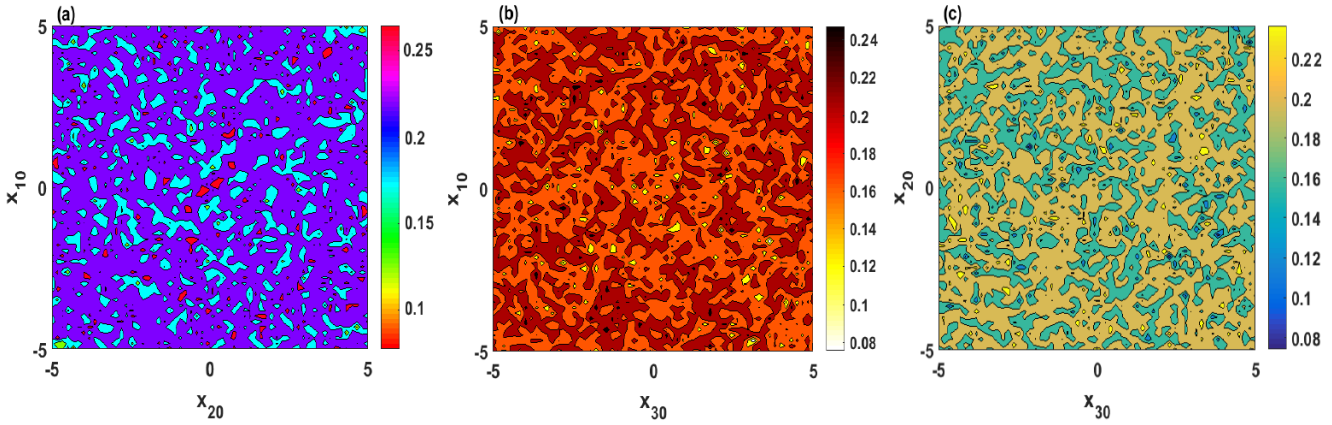


**Fig. 8.** LLE *versus* varying two of the initial values of case 2 with the parameters $\sigma = 12$, $\delta = 1.2$, $\beta = 0.1$: (a) $(x_{10}, x_{20}, 1)$; (b) $(x_{10}, 1, x_{30})$; (c) $(1, x_{20}, x_{30})$.

### 4.2 Sample entropy

Numerous measures that can be used to quantify the complexity of a dynamical system such as Approximate Entropy [29], Multiscale Entropy [30], and Sample Entropy [31]. However, we select Sample Entropy (SamEn) because it has the excellent properties of simplicity, robustness and fast calculation.

Suppose that the time series $(y_i, i = 0, 1, 2, \ldots, M-1)$ with a length of $M$, then the SamEn algorithm can be calculated by the following steps:

1) Reconstructing phase-space: for a given embedding dimension $m$ and time delay $\tau$, the reconstruction sequences are given by

$$Y_i = \{y_i, y_{i+\tau}, \ldots, y_{i+(m-1)\tau}\}, \quad y_i \in R^m, \tag{7}$$

where $i = 1, 2, \ldots, M - m + \tau$.

2) Counting the vector pairs: let $B_i$ be the number of vector $Y_j$, such that

$$d[Y_i, Y_j] \leq r, \quad i \neq j, \tag{8}$$

where $r$ is the tolerance parameter, and $d[Y_i, Y_j]$ is the distance between $Y_i$ and $Y_j$, which is defined by

$$d[Y_i, Y_j] = \max\{|y(i+k) - y(j+k)| : 0 \leq k \leq m-1\}. \tag{9}$$

3) Calculating probability: according to the obtained number of vector pairs, we can obtain

$$C_i^m(r) = \frac{B_i}{M - (m-1)\tau}, \tag{10}$$

then calculate the probability by

$$\phi^m(r) = \frac{\sum_{i=1}^{M-(m-1)\tau} \ln C_i^m(r)}{[M - (m-1)\tau]}. \tag{11}$$

4) Calculating SamEn: repeating the above steps we can obtain $\phi^{m+1}(r)$, then SamEn is given by

$$SamEn(m, r, M) = \phi^m(r) - \phi^{m+1}(r). \tag{12}$$

According to ref. [32], $m = 2$, $\tau = 1$ and $r = 0.1 \sim 0.2$ times standard deviation (SD) of the time series. In our experiment, we fix $m = 2$, $\tau = 1$ and $r = 0.2 \times SD$. SamEn of case 2 with one of the initial values varying in the range of $[-5, 5]$ is calculated, and the result is given in fig. 7(g)–(i). Moreover, fig. 9 shows the SamEn of case 2 with two of the initial values vary in the range of $[-5, 0]$ and $[0, -5]$ with step size of 0.03. It is worthwhile noting that SamEn of the well-known 3D dynamical systems, such as the Lorenz and Rössler systems, are $(0.1944 \pm 0.0074)$ and $(0.0930 \pm 0.0105)$, respectively [30]. Compared with these chaotic systems, case 2 has better complexity performance.

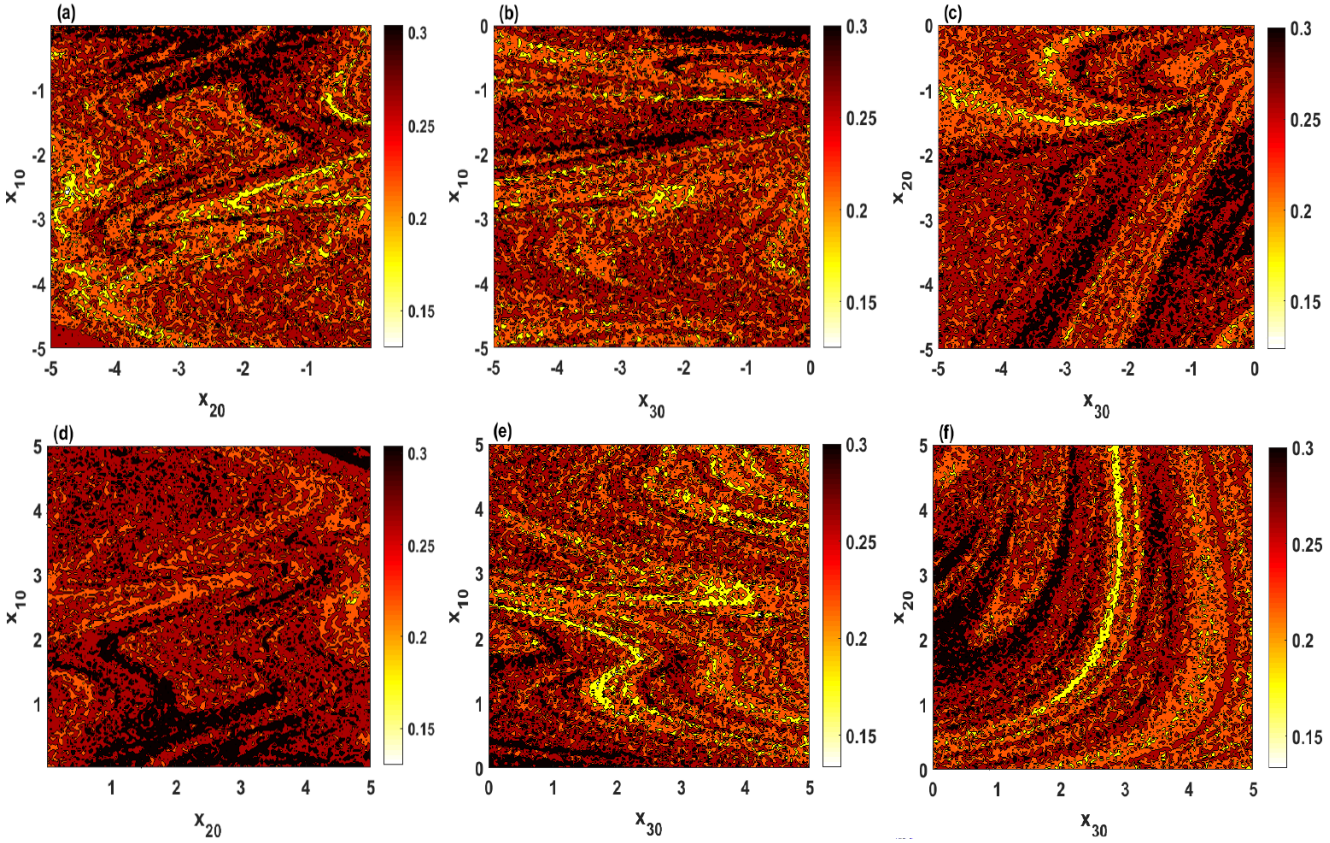


**Fig. 9.** SamEn *versus* varying two of the initial values of case 2 with the parameters $\sigma = 12$, $\delta = 1.2$, $\beta = 0.1$: (a), (d) $(x_{10}, x_{20}, 1)$; (b), (e) $(x_{10}, 1, x_{30})$; (c), (f) $(1, x_{20}, x_{30})$.

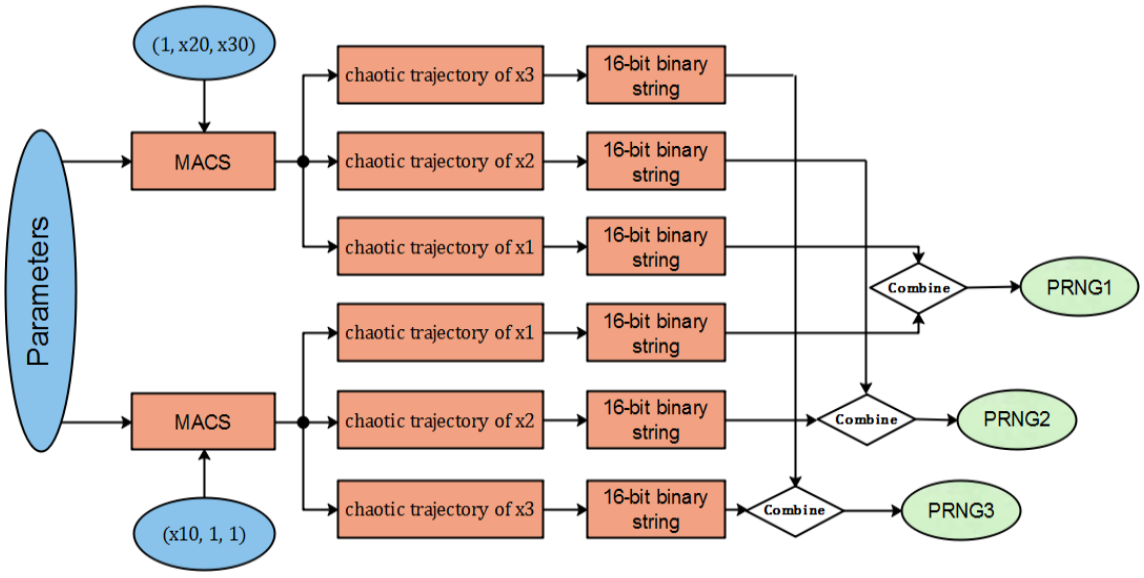


**Fig. 10.** The flowchart of generating PRNG.

### 4.3 Proposed algorithm and randomness tests

In order to generate a practical PRNG from a multi-stable chaotic system, a new algorithm based on case 2 of MACS is proposed. To achieve a fast throughput and facilitate hardware realization, 32-bit precision representation is assumed. The generation procedures of the PRNG are shown in algorithm 1 and fig. 10.

**Algorithm 1** The generation of chaos-based PRNG

**Input:** The parameters of case 2 that show coexisting chaotic attractors.

**for** $i = 1$ to 3 **do**
  **for** $x_{10}, x_{20}, x_{30} = 0$ to 5 **do**
    truncate the chaotic sequences $C_{1i}$ and $C_{2i}$ from $x_i$ when the initial values are $(5 - x_{10}, 1, 1)$ and $(1, 5 - x_{20}, x_{30} - 5)$, respectively;
    convert the floating numbers of $C_{1i}$ and $C_{2i}$ into a 32-bit binary using the IEEE-754-Standard;
    combine the last 16th digital number of the obtained binary string of $C_{1i}$ with the last 16th digital number of $C_{2i}$;
  **end for**
**end for**

**Output:** Three PRNG are generated from of $x_1$, $x_2$ and $x_3$.

**Table 3.** NIST-800-22 tests results of binary sequences of PRNG1, PRNG2 and PRNG3.

| Each sequence to be tested consist of 1000000 bits | | | | | |
|---|---|---|---|---|---|
| | NIST-800-22 tests | $p$-value (PRNG1) | $p$-value (PRNG2) | $p$-value (PRNG3) | Result |
| 1. | Block frequency ($m = 128$) | 0.3961 | 0.0562 | 0.3807 | Random |
| 2. | Frequency (Monobit) | 0.0293 | 0.3360 | 0.3370 | Random |
| 3. | Discrete Fourier transform | 0.0820 | 0.2588 | 0.7603 | Random |
| 4. | Approximate entropy ($m = 10$) | 0.1774 | 0.2519 | 0.9730 | Random |
| 5. | Cumulative sums (Forward) | 0.0136 | 0.2309 | 0.3302 | Random |
| 6. | Serial-1 ($m = 16$) | 0.8633 | 0.0985 | 0.5819 | Random |
| 7. | Runs | 0.6105 | 0.5358 | 0.4151 | Random |
| 8. | Longest run of ones | 0.3266 | 0.1515 | 0.6656 | Random |
| 9. | Overlapping template ($m = 9$) | 0.1841 | 0.7277 | 0.1708 | Random |
| 10. | Non-overlapping template ($m = 9$) | 0.5007 | 0.5600 | 0.5270 | Random |
| 11. | Linear complexity | 0.2862 | 0.2793 | 0.8425 | Random |
| 12. | Binary matrix rank | 0.7381 | 0.4904 | 0.6212 | Random |
| 13. | Lempel-ziv compression | 0.6281 | 0.8964 | 0.7509 | Random |
| 14. | Random excursions | 0.7935 | 0.4963 | 0.5637 | Random |
| 15. | Random excursions variant | 0.6248 | 0.4500 | 0.5827 | Random |
| 16. | Universal statistical | 0.1066 | 0.0345 | 0.6940 | Random |

Several statistical tests can be employed to test the randomness of PRNG. Our experiment use the highest standards of statistical packages which is NIST-800-22. The NIST-800-22 consists of 16 empirical statistical tests that provide true evaluation for the randomness of PRNG. Each test is developed to detect the non-random areas of a binary sequence from different sides, and then derive a $p$-value. When the obtained $p$-value is $> 0.01$, we then conclude that the binary sequence has pass the statistical test; otherwise, the binary sequence is non-random.

According to algorithm 1, we can obtain three PRNG from the trajectory of $x_1$, $x_2$, and $x_3$ when the parameters are considered as input. For $\sigma = 12$, $\delta = 1.2$ and $b = 0.1$, table 3 lists the NIST-800-22 results for PRNG1, PRNG2 and PRNG3 when the generated binary sequences are of length 1000000 bits. It is obvious that the three PRNG can pass all the statistical tests.

## 5 Conclusions

A novel 3D chaotic system has been reported here with different characteristics. This proposed system can have no equilibrium, an unstable equilibrium, and a stable equilibrium. That means, there exist two kinds of attractors, self-excited chaotic attractor with an unstable equilibrium and hidden chaotic attractor with no equilibrium or a stable equilibrium. Moreover, two, three and four coexisting attractors are obtained by choosing appropriate parameters including periodic with periodic attractors, periodic with chaotic attractors, and chaotic with chaotic attractors. Due to the fact that such chaotic system constructed in this paper not only possesses two kinds of attractors but also has complicated dynamic properties including high complexity performance, and highly sensitivity to its initial values and parameters, it could be utilized in chaos-based cryptographic applications including chaos-based PRNG, secure communication, and image encryption. Therefore, we used chaos-based PRNG as an example to further demonstrate the effectiveness of the new system in practical application. Performance test results show that the new chaotic system is appropriate for cryptographic applications.

## References


1. E.N. Lorenz, J. Atmos. Sci. **20**, 130 (1963).
2. O.E. Rössler, Phys. Lett. A **57**, 397 (1976).
3. J.C. Sprott, Phys. Rev. E **50**, R647 (1994).
4. G. Chen, T. Ueta, Int. J. Bifurc. Chaos **9**, 1465 (1999).
5. S. Banerjee, S.K. Palit, S. Mukherjee, M. Ariffin, L. Rondoni, Chaos **3**, 033105 (2016).
6. L. Rondoni, M.R.K. Ariffin, R. Varatharajoo, S. Mukherjee, S.K. Palit, S. Banerjee, Opt. Commun. **387**, 257 (2017).
7. S. Theesar, Jeeva Sathya, Santo Banerjee, P. Balasubramaniam, Nonlinear Dyn. **70**, 1977 (2012).
8. Papri Saha, Santo Banerjee, A. Roy Chowdhury, Phys. Lett. A **326**, 133 (2004).
9. G.A. Leonov, N.V. Kuznetsov, Int. J. Bifurc. Chaos **23**, 1330002 (2013).
10. Alexander N. Pisarchik, Ulrike Feudel, Phys. Rep. **540**, 167 (2014).
11. F.T. Arecchi, R. Meucci, G. Puccioni, J. Tredicce, Phys. Rev. Lett. **49**, 1217 (1982).
12. J.C. Sprott, X. Wang, G. Chen, Int. J. Bifurc. Chaos **23**, 1350093 (2013).
13. C. Li, J.C. Sprott, Int. J. Bifurc. Chaos **24**, 1450131 (2014).
14. J. Kengne, Z.T. Njitacke, H.B. Fotsin, Nonlinear Dyn. **83**, 751 (2016).
15. G. Wang, F. Yuan, G. Chen, Y. Zhang, Chaos **28**, 013125 (2018).
16. Guanrong Chen, *Chaotification via feedback: the discrete case*, in *Chaos Control* (Springer, Berlin, Heidelberg, 2003) p. 159.
17. Hongjie, Yu, Liu Yanzhu, Phys. Lett. A **314**, 292 (2003).
18. J.C. Sprott, S. Jafari, A.J.M. Khalaf, T. Kapitaniak, Eur. Phys. J. ST **226**, 1979 (2017).
19. Sajad Jafari, Viet-Thanh Pham, Tomasz Kapitaniak, Int. J. Bifurc. Chaos **26**, 1650031 (2016).
20. Gonzalo Alvarez, Shujun Li, Int. J. Bifurc. Chaos **16**, 2129 (2006).
21. Santo Banerjee, Chaos, Solitons Fractals **42**, 745 (2009).
22. Santo Banerjee, Sumona Mukhopadhyay, Lamberto Rondoni, Opt. Lasers Eng. **50**, 950 (2012).
23. H. Natiq, N. Al-Saidi, M.R.M. Said, A. Kilicman, Eur. Phys. J. Plus **133**, 6 (2018).
24. H. Natiq, S. Banerjee, S. He, M.R.M. Said, A. Kilicman, Chaos, Solitons Fractals **114**, 506 (2018).
25. Zhongyun Hua, Yicong Zhou, Inf. Sci. **339**, 237 (2016).
26. Santo Banerjee, D. Ghosh, A. Roy Chowdhury, Phys. Scr. **78**, 015010 (2008).
27. G.C. Layek, *An Introduction to Dynamical Systems and Chaos* (Springer, New Delhi, 2015).
28. C.K. Volos, I.M. Kyprianidis, I.N. Stouboulos, Int. J. Multime. Intell. Secur. **1**, 320 (2010).
29. Steven M. Pincus, Proc. Natl. Acad. Sci. **88**, 2297 (1991).
30. M. Costa, C.K. Peng, A.L. Goldberger, J.M. Hausdorff, Physica A **330**, 53 (2003).
31. J.S. Richman, J.R. Moorman, Am. J. Physiol.-Heart Circ. Physiol. **278**, H2039 (2000).
32. F. Kaffashi, R. Foglyano, C.G. Wilson, K.A. Loparo, Phys. D **237**, 3069 (2008).